Thermodynamic and kinetic properties of surface dislocations on Au(001) from atomistic simulations

Chun-Wei Pao
Department of Mechanical and Aerospace Engineering, Princeton University, Princeton, New Jersey 08544, USA

David J. Srolovitz
Department of Physics, Yeshiva University, New York, New York 10033, USA

Henny W. Zandbergen
National Centre for HREM, Kavli Centre of Nanoscience, Delft University of Technology, 2628 AL Delft, The Netherlands
(Received 2 January 2007; published 3 May 2007)

We examined the thermodynamic and kinetic properties of surface dislocations on the Au (001) surface using atomistic simulations based on a modified embedded atom potential that was optimized for Au surfaces. Two different surface dislocations are obtained, containing five displaced atomic columns (type I) or three displaced atomic columns (type II). Both configurations are more stable than adatoms on the surface and type I is more stable than type II surface dislocation. The energy of the surface containing type I surface dislocations decreases with decreasing dislocation spacing, while that containing type II surface dislocations exhibits a minimum at a particular dislocation spacing. The surface stress of surfaces with type I surface dislocations surprisingly increases with decreasing surface dislocation spacing, while the surface stress decreases with decreasing dislocation spacing on surfaces containing type II surface dislocations. We also calculated the activation energies for surface dislocation migration in directions perpendicular and parallel to the surface dislocation line using a string method. The activation energies of both perpendicular and parallel motions are similar, and therefore a surface dislocation can move both parallel and normal to itself. This has been confirmed experimentally. We also found that type II surface surface dislocation corresponds to a metastable structure through which the type I surface dislocation must pass as it migrates perpendicular to its line direction.

DOI: 10.1103/PhysRevB.75.195405 PACS number(s): 68.55.−a, 68.35.Md, 68.35.Gy, 68.35.Fx

I. INTRODUCTION

Surface reconstructions of Au, Pt, and Ir have been reported on several low index surfaces, including (001) and (111).[1–12] The fully reconstructed surfaces have different surface atomic packings and densities compared with the unreconstructed surfaces. The reconstruction of the (001) surface into a (5×1) structure, with quasihexagonal surface atomic packing, has long been known; the atomic density of this surface is 20% larger than the corresponding unreconstructed surface.[1–4,7,8,10,12] The {111} surface shows a reconstruction in which an extra column of atoms is added each 22 columns. Due to this addition to the local stacking, the top layer changes from faced center cubiclike (*ABC*) to hexagonal closed packinglike (*ABA*), resulting in a network of corrugated stripes with different patterns.[5,6,9–11] These fully reconstructed surfaces exist when the surface is in equilibrium. However, during film growth and evaporation processes, the surface is commonly far from equilibrium and hence the surface structure may be quite different from the equilibrium reconstructed surfaces.

Recent studies have revealed that the structure of nonequilibrium Au (001) surfaces can be very dynamic. Labayen *et al.*[13,14] reported mobile isolated strings on Au (001) surface that can move either perpendicular to or along the string direction. Zandbergen *et al.*,[15] using high resolution electron microscopy, observed during the evaporation of a Au film that Au adatoms are collectively injected from the surface into the terrace and these form highly mobile surface dislocations on Au (001). The surface dislocation was observed to move back and forth within the terrace. These studies showed that an extra ⟨110⟩ column of atoms on the (001) surface squeezed into the surface (terrace) to form a surface dislocation (string). Two distinct types of surface dislocations were observed. The first consists of five atomic columns displaced along the ⟨110⟩ direction with all five columns also displaced normal to the surface plane and the center atomic column displaced normal to the surface most of all (single ridge). The second consisted of three atomic columns displaced along the ⟨110⟩ direction with all three columns also displaced normal to the surface plane and the center atomic column displaced normal to the surface less than the other two (double ridge). The surface atomic packing around the surface dislocation (string) center is quasihexagonal for both types. The first type of surface dislocation (single ridge) has the same structure as the elementary unit cell of the equilibrium (5×1) reconstruction. Therefore, (001) surfaces with this dynamic surface structures appear as partially reconstructed surfaces.

The existence of surface dislocations provides insights into several important surface phenomena on metal surfaces. First, since one extra column of atoms is injected into the surface to form a surface dislocation, it should be expected to introduce a compressive stress and, therefore, significantly reduce the tensile surface stress of the Au (001) surface. This is a possible explanation for the compressive stress in many

continuous films.[16,17] Second, since these surface dislocations are highly mobile in directions both perpendicular and parallel with the dislocation line direction, surface dislocations can provide an important mechanism for surface mass transport—in addition to classic mechanisms such as atomic hopping and exchange. Surface mass transport via surface dislocation is potentially very efficient because the atomic motion is highly correlated and wavelike. However, the influence of surface dislocations on surface thermodynamic properties (e.g., surface energy and surface stress) and the migration of these surface dislocations remain largely unknown.

In the present study, we focus on the thermodynamic and kinetic properties of surface dislocations on Au (001). We examine the stability of different surface dislocation structures and how surface dislocations modify the surface energy and surface stress. We also examine how surface dislocations move on the surface. In the next section, we describe the theoretical methods employed in the present study. Then, in the following two sections, we examine two stable surface dislocation structures and their influence on surface thermodynamics. Next, we examine surface dislocation dynamics and kinetics, including determination of the transition path and activation energy associated with surface dislocation motion. Finally, we summarize our results and discuss their implications for several surface processes.

II. SIMULATION METHODS

Our main tool in the analysis of surface dislocations used in this study is (both static and dynamic) atomistic simulation. Since our focus is the Au (001) surface, it is important to employ an interatomic potential which can properly replicate the surface properties of Au. There have been a number of embedded atom method-type potentials for Au which generate the (5×1) reconstruction of Au (001).[18–21] However, these potentials fail to replicate the surface structures observed by Labayen *et al.*[13] and Zandbergen *et al.*,[15] e.g., the instability of the (1×1) unreconstructed surface at finite temperature (i.e., $T>0$ K). Therefore, the present studies were performed using the modified embedded atom method potential (MEAM) for Au,[22] which replicates the finite temperature (5×1) reconstruction on Au (001) [the MEAM potentials also provide a reasonable description of the (001) surfaces of several transition metals].[23]

To determine the stable structures of the surface dislocations, we applied both classical molecular-dynamics simulations (MD) and conjugated gradient energy minimizations. The simulation cell adopted here is periodic in both the $X(\langle 1\bar{1}0\rangle)$ and $Y(\langle 110\rangle)$ directions, while the $Z(\langle 001\rangle)$ direction (perpendicular to the surface) is not periodic, in order to simulate free surfaces. We began by placing an effectively infinitely long atom column on the (001) surface, aligned along the $\langle 110\rangle$ direction and minimized the energy of the system using a conjugate gradient method. After this $T=0$ structure relaxation, this atomic column remained on the surface. Hence, the adatom column is either stable or, at least, metastable at $T=0$.

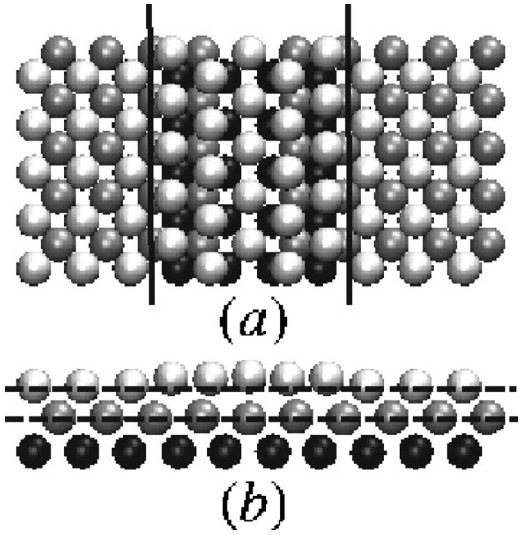

FIG. 1. The structure of type I surface dislocation. Only the top three (002) planes of atoms are shown, where the shading indicates the plane (where the atoms become darker with increasing atomic plane number from the surface—this shading is adopted throughout this paper). (a) The view from the top ($\langle 001\rangle$) and (b) along the side ($\langle 110\rangle$). In (a), the two thick dark lines delimit the surface dislocation core and separate the hexagonal surface atomic packing from the unreconstructed (001) (1×1) surface atomic packing. In (b), the dark dashed lines denote the positions of the first two (002) atomic planes in the surface without a surface dislocation.

In the present study, we were able to obtain two different surface dislocation structures by performing finite temperature MD simulations. The resultant dislocations had structures which matched the type I and II surface dislocations seen in experiment (see Figs. 1 and 2). Two types of finite temperature simulations were performed. In the first, we artificially injected the adatom column into the surface and then performed the MD simulations. In the second, we simply heated the system with the adatom column atop the (001) surface. In the first case, both type I and type II surface

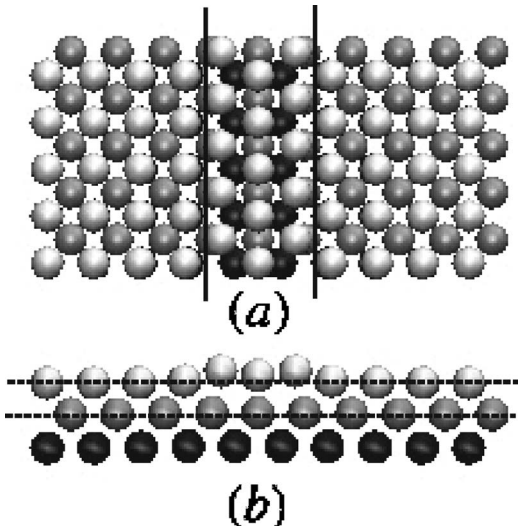

FIG. 2. The structure of type II surface dislocation, as per Fig. 1.

dislocations were stable at 300 K. In the second case, we heated the sample with the adatom column on the surface to 900 K and then gradually cooled back to low temperature. In this case, we only observed type II surface dislocation. We discuss the structure of these dislocations in the next section.

Using these dislocation configurations, we calculated the change in surface energy and surface stress as a function of spacing between surface dislocations (by changing simulation cell length along the $\langle 1\bar{1}0\rangle$ direction) using conjugate gradient method minimizations. To calculate the surface stress, we measured the energies of systems with the same surface structures and different system slab thicknesses (along $\langle 001\rangle$) under the same surface strain ε_{xx} (straining along $\langle 1\bar{1}0\rangle$) to obtain the change in surface energy associated with the surface strain. The slope of the surface energy as a function of strain is the surface stress (interested readers can refer to Pao *et al.*[24] for more details).

In order to determine the kinetics of surface dislocation motion, we applied the minimum-energy path approach to determine the activation energy for migration, as well as the transition path using the string method developed by E *et al.*[25] In the string method, we calculate the minimum-energy path by connecting the initial and final N-atom configurations by a string of states in the $3N$-dimensional configuration space. In practice, this is done by discretizing the string into a sequence of system replicas, and then evolving the string along the normal to the string tangent. The minimum-energy path is found when the force acting on the string is purely tangent to the string. Since experimental observations show that surface dislocations can migrate both parallel and perpendicular to the dislocation line direction, we examined a series of different types of motion along each, which will be addressed further in Sec. V.

In all of the string method calculations, we employed 120 system replicas to represent the "string" connecting the initial and final configurations. The boundary conditions of the simulation cells for all these calculations are the same as above. The dimensions of the simulation cell in the *X*-*Y* plane were 29×86 Å^2 for perpendicular motion, while for all other motions, the simulation cell was set to 58×46 Å^2 in order to minimize finite-size effects. The energies of the system replicas very close to the initial and final configurations (within five system replicas) are slightly lower than the initial and final configurations (by up to 0.002 J/m^2) due to the complicated energy landscape.[26] Therefore, we start from these replicas to plot the energy landscape along the minimum-energy path and calculate the activation barrier of the reaction pathway as the difference between the highest system energy along the pathway and the energy of the starting point of the minimum-energy path.

III. SURFACE DISLOCATION STRUCTURE

As described above, two different types of stable surface dislocation structures are obtained by applying two different relaxation methods. Figure 1(a) shows type I surface dislocation viewed normal to the surface (i.e., the $\langle 001\rangle$ direction or top view). The core of type I surface dislocation consists of five $\langle 110\rangle$ atomic columns displaced from another along $\langle 110\rangle$ to form a quasihexagonal surface atomic packing (the core is delineated by two thick dark lines for clarity). Figure 1(b) shows that type I surface dislocation viewed along the $\langle 110\rangle$ direction (i.e., side view). In this view, we see that the surface layer buckles around the dislocation core as a result of the injection of an extra atomic column to form the surface dislocation. The structure of type I surface dislocation is in fairly good agreement with high-resolution electron microscopy (HREM) images (viewed along $\langle 110\rangle$, the side view) obtained by Zandbergen *et al.*[15] and is also consistent with the "single-ridge" configuration observed by Labayen *et al.*[13] (viewed along $\langle 001\rangle$, the top view).

The relaxed structure of type II surface dislocation is shown in Fig. 2. The core of type II surface dislocation consists of three displaced $\langle 110\rangle$ atomic columns that are shifted relative to one another along the column direction to form a narrow quasihexagonal surface atomic packing (as delineated by the thick dark lines in the figure). From the side view, shown in Fig. 2(b) (viewed along the $\langle 110\rangle$ direction), we see that the two atomic columns on either side of the dislocation core center are slightly elevated. The main difference between the structures of the cores of the two surface dislocations is the core width (narrower in type II than in type I). The structure of type II surface dislocation obtained in the present study is again in good agreement with the HREM images of Zandbergen *et al.*[15] (the side view) and the "double-ridge" configuration observed by Labayen *et al.*[13] (the top view).

IV. SURFACE ENERGY AND SURFACE STRESS

To what extent the formation of surface dislocations affects surface thermodynamic properties is largely unknown. In this section, we examine the effects of both types of surface dislocations on the surface energy and surface stress as a function of surface dislocation spacing.

The surface energy γ as a function of surface dislocation spacing d is shown in Fig. 3. The smallest value of d for which data are shown in Fig. 3 corresponds to the period of the equilibrium (5×1) reconstructed surface, i.e., $d=3.54a_0$. Figure 3 shows that the surface energy is a function of surface dislocation spacing. However, the effects of these surface dislocations and adatom columns on surface energy do not change the surface energy by more than 10%. For type I surface dislocation, the surface energy decreases with decreasing surface dislocations spacing [until the (5×1) structure is achieved]. This attractive interaction is consistent with experimental observations.[13] Type II surface dislocations attract one another at large separation and repel at small separations, leading to an equilibrium separation that is larger than for type I surface dislocations. On the other hand, the simulation data suggest that the adatom columns repel one another at all separations.

The simulation data also suggest that the Au (001) surfaces with type I surface dislocations exhibit lower energies than their unreconstructed, type II containing or adatom column-containing counterparts. The fact that the Au (001) surface containing either type of surface dislocation has

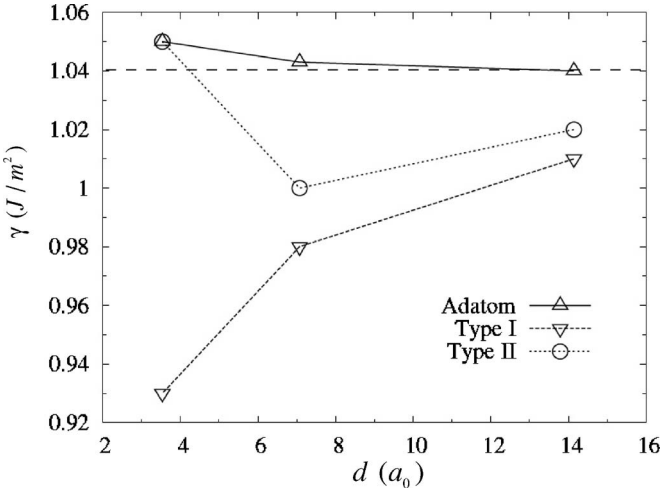

FIG. 3. Surface energy γ versus surface dislocation spacing d (in units of the bulk Au lattice parameter a_0=4.08 Å). The dashed line represents the surface energy of the unreconstructed (001) surface (i.e., 1.04 J/m^2). Also shown for completeness is the surface energy corresponding to the situation where the column of adatoms sits atop a (001) terrace.

lower energy than the unreconstructed surface explains why both types of surface dislocations are experimentally observed by both Labayen *et al.*[13] and Zandbergen *et al.*[15]

Figure 4 shows the surface stress f as a function of surface dislocation spacing (adatom column spacing) d. The dashed line in the figure denotes the surface stress of an unreconstructed (001) surface. Note again that the smallest d reported is $d=3.54a_0$, the spacing between type I surface dislocations in the equilibrium (5×1) surface reconstruction. As shown in Fig. 4, all three types of surface defects considered here have a pronounced effect on the surface stress—changing the surface stress by as much as 125%. Surprisingly, this effect is smallest for the adatom column. In all cases, decreasing the spacing between the defects (i.e., increasing their surface density) increases the magnitude of the

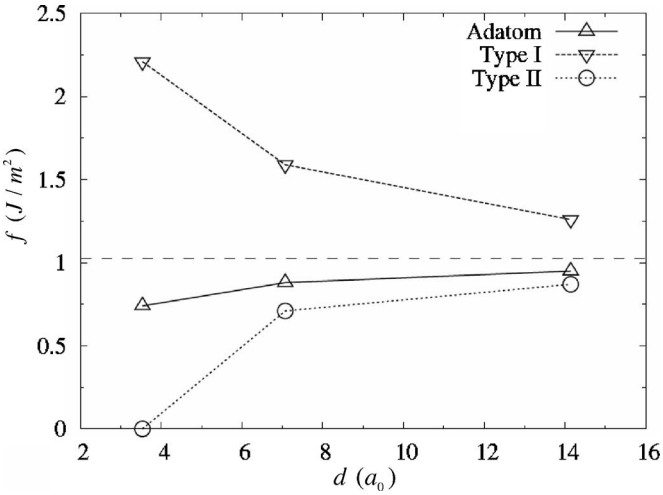

FIG. 4. Surface stress f vs surface dislocation spacing d (with units of bulk lattice parameter of Au, 4.08 Å). The dashed line shown is the surface stress of a singular (001) surface (1.02 J/m^2).

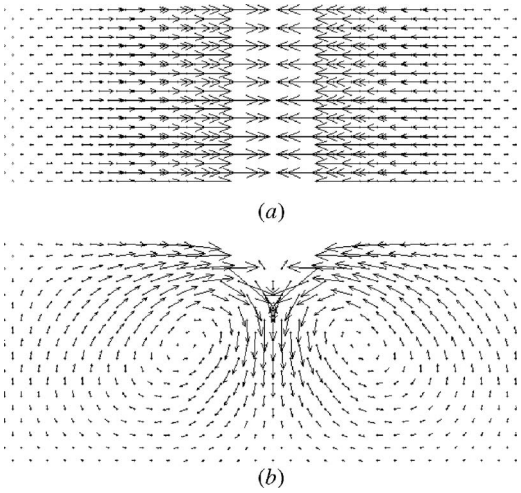

FIG. 5. The displacement field associated with type I surface dislocation, as viewed from (a) the top (along the ⟨001⟩ direction) and (b) the side (along the ⟨110⟩ direction). In both figures, displacements larger than 0.05 Å (i.e., atoms near the dislocation core region) are not shown.

change. The other big surprise here is that while type I surface dislocations lead to an increase in the tensile surface stress, type II surface dislocations produce a large decrease in the tensile surface stress. At first glance, we would expect that surface dislocations would decrease the tensile surface stress since they are created by forcing an extra column of atoms into a complete (001) plane.

In order to understand why type I and II surface dislocations have opposite effects on the surface stress, we plot the displacement field of the these surface dislocations, as shown in Figs. 5 and 6. These displacement fields are obtained by calculating the difference in atomic positions between the relaxed atomic configurations with surface dislocations and an unreconstructed (001) surface. From Fig. 5, we can see

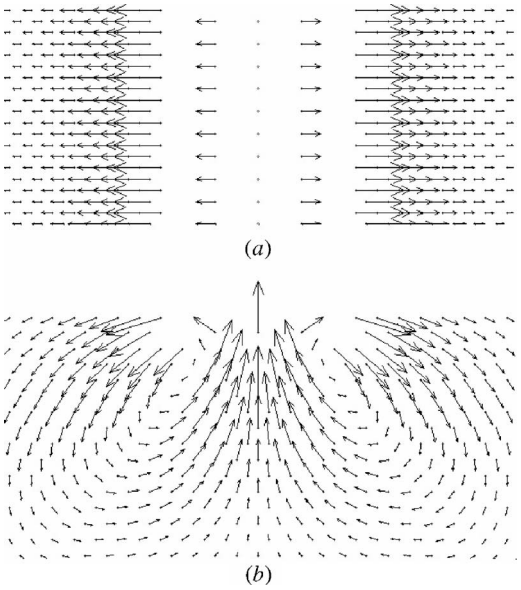

FIG. 6. The displacement field associated with type II surface dislocation, as per Fig. 5.

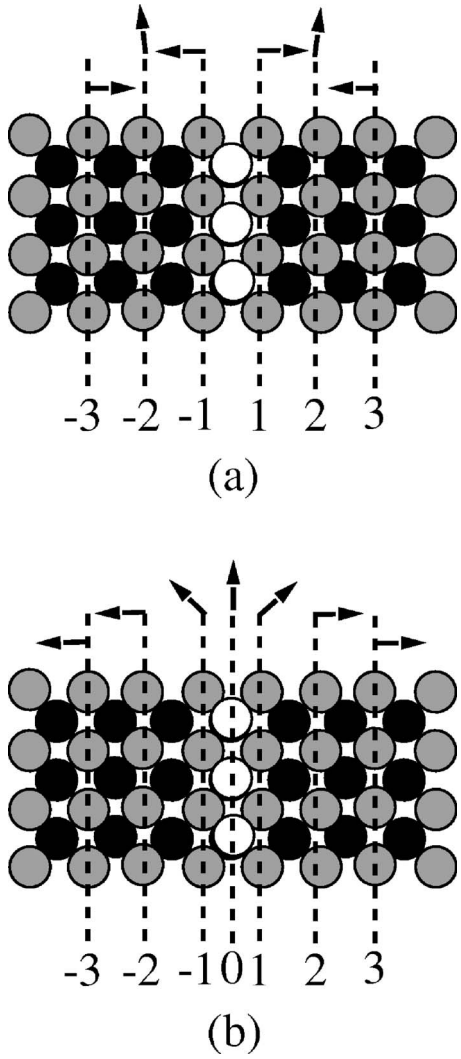

FIG. 7. The directions of surface atom column displacements near the center of (a) type I surface dislocation and (b) type II surface dislocation. White atoms denote the injected atom column that forms the center of the surface dislocation. Gray atoms denote the surface atoms and black atoms denote the atoms in the plane directly below the surface. Both figures are viewed along the ⟨001⟩ direction (top view).

that the introduction of type I surface dislocation pulls the neighboring surface atoms toward the surface dislocation. This makes the surface stress more tensile. On the other hand, examination of Fig. 6 shows that the atoms neighboring type II surface dislocation are pushed away from the surface dislocation. The creation of a compressive stress that added to the intrinsic tensile stress of the unreconstructed surface leads to a decrease in the tensile stress. Interestingly, when type II surface dislocations are $d=3.54a_0$ apart, the surface stress is almost zero.

We can further understand why type I surface dislocation attracts neighboring surface atoms and type II surface dislocation repels neighboring surface atoms by considering the atomic packing of both types of surface dislocations. Figure 7 shows the directions of surface atomic displacements that occur upon the injection of the extra atomic column (atoms colored in white) for both types of surface dislocations. The surface atoms (colored in gray) linked by the same dashed line in the figure displace in the same directions and by the same amount. In Fig. 7(a), we see that when the extra atom column is injected (moves into the plane of the figure) to form type I surface dislocation, the atomic columns immediately neighboring the extra atom column, columns +1 and −1, displace in the right and left directions, respectively. The atomic columns +2 and −2 shift primarily upward [as shown in Fig. 7(a)], causing atom columns +3 and −3 to shift toward the injected atom column (i.e., the left and right directions) to avoid an increase in the interatomic distance between atoms in coloumns +3 and +2 (−3 and −2). The inward shifts of atom columns +3 and −3 set up a long-range elastic field that shifts surface atoms further out toward type I surface dislocation. It is this long range inward shift that makes the surface stress more tensile. It is important to note that one way the surface atomic plane accommodates the net motion of the atoms outside the core toward the core is to buckle into the direction orthogonal to the surface, as seen in Fig. 1(b). This occurs because each atom moves such as to maintain the correct local electron density, as argued previously to explain surface relaxation effects.[27]

The surface atomic displacements associated with type II surface dislocation are quite different from that found for type I surface dislocation. Figure 7(b) shows the displacement field associated with injecting the atom column (position 0) into the Au (001) surface plane. In this case, the extra atom column 0 shifts upward on injection. This causes atom columns +1 and −1 to move both up and right and up and left, respectively. Atom columns +2 and −2 (unlike those in type I surface dislocation case) shift in the right and left directions away from the injected atom column with almost no displacement parallel to the dislocation line direction. This outward motion of columns +2 and −2 forces atom columns +3 and −3 outward. This continues as we move further away from the center of the surface dislocation, and hence this creates a compressive strain on the surface away from the surface dislocation. Hence, the introduction of type II surface dislocation creates an additional compressive surface stress that decreases the overall surface stress from the tensile surface stress found in the unreconstructed Au (001) (1×1) structure.

V. SURFACE DISLOCATION MIGRATION

In this section, we examine how surface dislocations move. We determine the transition path between equivalent dislocation positions and calculate the activation barriers for motion both perpendicular and parallel to the dislocation line. Based on experimental observations, we proposed five possible migration mechanisms: perpendicular, canted, parallel I, parallel II, and parallel III, as shown in Fig. 8. We introduce a reaction coordinate parameter α which identifies the dislocation position along the reaction path. If we break the reaction path into N_0 steps, then α takes on values N/N_0, where $0\leqslant N\leqslant N_0$ is the index of the replica along the minimum-energy path. Therefore, $\alpha=0$ denotes the initial configuration, while 1.0 denotes the final configuration. Since the results above suggest that the most stable surface

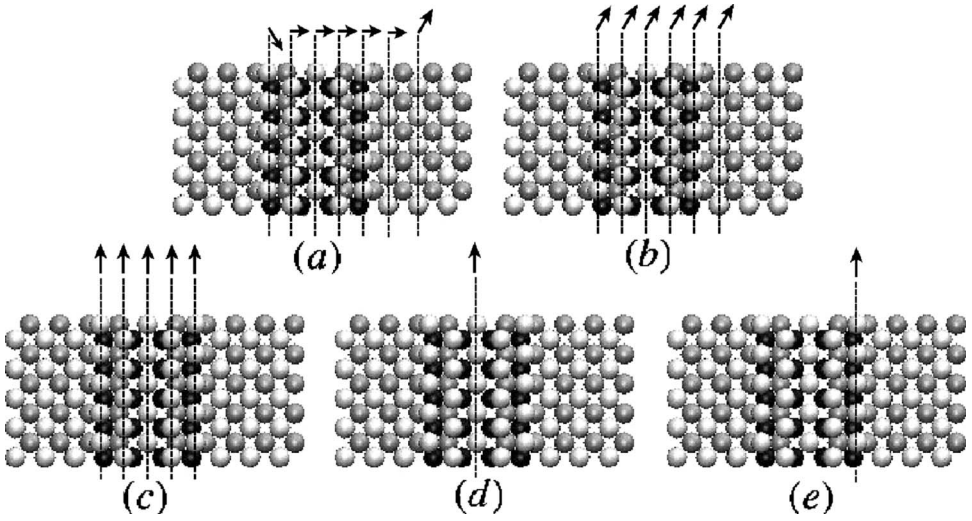

FIG. 8. The possible atomic motions that lead to the migration of the surface dislocation along directions perpendicular to and parallel with the dislocation line. The arrows show the directions of the motion of the light gray atoms (surface atoms) in the same column. We label the types of motion as (a) perpendicular, (b) canted (i.e., a hybrid of perpendicular and parallel motions), (c) parallel I (where all five columns move parallel to the line direction), (d) parallel II (i.e., only the center atom column moves), and (e) parallel III (where only the atomic column at the edge of the core moves).

dislocation is of type I, we choose the initial and final configurations to be adjacent type I surface dislocation configurations.

As seen in Fig. 8(a), a unit step of the surface dislocation perpendicular to its line direction corresponds to a translation by $2d_{\langle 1\bar{1}0\rangle}$ along the $\langle 1\bar{1}0\rangle$ direction, where $d_{\langle 1\bar{1}0\rangle}$ denotes the nearest-neighbor distance in Au, whereas in the canted motion [shown in Fig. 8(b)], all of the atoms in the core shift both perpendicular and parallel to the dislocation line by a distance $d_{\langle 1\bar{1}0\rangle}$ in each direction (i.e., along the $\langle 001\rangle$ direction by a distance a_0, where $a_0=\sqrt{2}d_{\langle 1\bar{1}0\rangle}$ denotes the lattice parameter of Au). As described in Sec. II, the simulation cell size in the X-Y plane for the perpendicular motion study is 29×86 Å^2, while for the canted (and all other types of) motion, the simulation cell is 58×46 Å^2. To ensure that the size of the simulation cell does not effect our computation of the transition path and activation energy, we also simulated the perpendicular motion in the larger simulation cell. We found that going to the larger simulation cell size has no significant effect on the computed activation energy. Figure 9 shows the calculated minimum-energy paths for both the perpendicular and canted motions of the surface dislocation. Table I shows that the activation energy for the canted motion, 0.168 eV/Å, is considerably larger than for the perpendicular motion, 0.076 eV/Å. Hence, we conclude that the perpendicular motion mechanism is the dominant mechanism by which the surface dislocation translates. Unlike in the canted motion, when the dislocation line moves perpendicular to itself, there are three energy maxima (see Fig. 9) and two metastable minimum-energy positions.

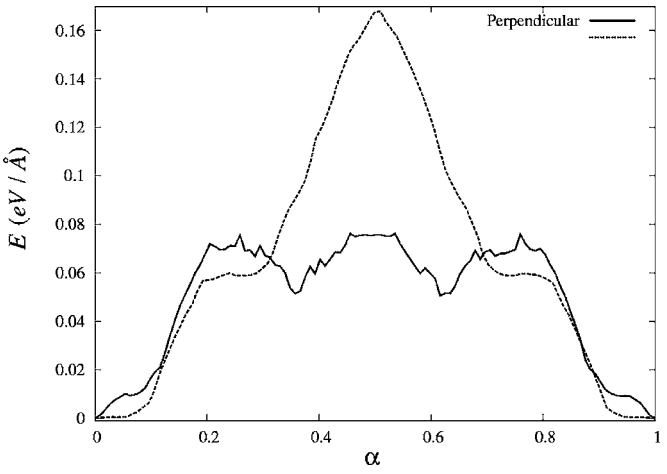

FIG. 9. The minimum-energy path for the pure perpendicular and canted of the migration of the surface dislocation with pure perpendicular and canted motions. "Perpendicular" and "canted" correspond to Figs. 8(a) and 8(b), respectively.

Figure 10 shows seven representative images of the atomic configuration during the perpendicular motion of the surface dislocation. The left and right arrows above each image indicate the locations of the center of the surface dis-

TABLE I. The calculated activation energy of surface dislocation migration on Au (001) surfaces. The activation energy is defined as the energy differences between $\alpha=0$ and the highest energy shown in both Figs. 9 and 11. The migration types are defined in Fig. 8.

Migration type	Activation energy (eV/Å)
Perpendicular	0.076
Canted	0.168
Parallel I	0.117
Parallel II	0.078
Parallel III	0.065

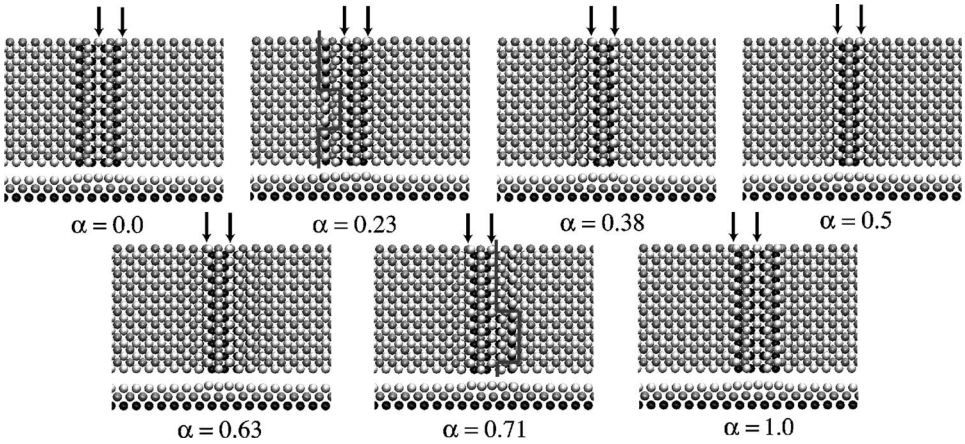

FIG. 10. Representative images during the perpendicular surface dislocation migration. In each pair of images, the upper and lower ones correspond to top and side views, respectively. α denotes the reaction coordinate. The two arrows above each figure highlight the location of the dislocation center at α=0 (left arrow) and the α=1.0 (right arrow). The thick gray lines shown in the α=0.23 and 0.71 images highlight the location of kinks along the dislocation line.

location before and after the single perpendicular motion dislocation step. Combining Figs. 9 and 10, we see that α =0.0 and 1.0 are the initial and final states, α=0.5 is the middle of the transition, α=0.38 and 0.63 are the two metastable transition states, and α=0.23 (α=0.71) correspond to the transition states between the initial (final) state and the metastable transition states (α=0.38 and 0.63). The metastable configurations (α=0.38 and 0.63) correspond to type II surface dislocation structure. That these states correspond to type II surface dislocation structure implies that type II surface dislocation, or the double-ridge type in Labayen *et al.*[13] is probably just a metastable transition state during the perpendicular migration of the surface dislocation.

The thick gray line in the α=0.23 image in Fig. 10 highlights the double kink formed during the transition from the initial configuration to the metastable transition state (α =0.38). The atomic configurations above and below the double kink pair correspond to the stable type I surface dislocation structure. Between the two kinks, on the other hand, the structure is that of type II surface dislocation (i.e., the metastable structure). The same description also pertains to the α=0.71 state, which is between α=0.63 metastable state and the α=1 final state. The present results indicate that the motion of the surface dislocation, perpendicular to itself, occurs by a double kink nucleation and kink propagation mechanism. The interesting thing here is that the kink mechanism operates between stable and metastable states and does not operate between the two metastable states (i.e., note that there is no double kink present at α=0.5).

Figures 8(c)–8(e) show three different possible mechanisms for surface dislocation migration in the direction parallel to itself. In parallel I motion, the entire five ⟨110⟩ atomic column core of the surface dislocation shifts upward by $1d_{\langle 1\bar{1}0\rangle}$. In both parallel II and III motions, on the other hand, only one atomic column of the surface dislocation is involved: the center column of the surface dislocation shifts upward by $1d_{\langle 1\bar{1}0\rangle}$ in parallel II motion, whereas the leading atomic column in the dislocation core shifts upward $1d_{\langle 1\bar{1}0\rangle}$ in parallel III motion.

The calculated minimum-energy paths for the parallel motions are shown in Fig. 11. Combined with Table I, we find that both parallel II and III motions have lower activation energies. This is not surprising because in these mechanisms only one ⟨110⟩ atomic column is involved, while in parallel I motion, all five ⟨110⟩ atomic columns of the surface dislocation shift. Compared with the activation energy for perpendicular motion (see Table I), we find that parallel II motion and parallel III motion exhibit similar activation energies (0.078 and 0.065 eV/Å, respectively) and that the activation energies for these parallel motions are similar in magnitude to that of perpendicular motion (0.076 eV/Å). Although it is tempting to say that parallel III motion should occur faster than any other type of surface dislocation migration, it is probably beyond the accuracy of the interatomic potential to distinguish between the perpendicular parallel II and parallel III activation energies (i.e., they differ by only ~0.01 eV/Å).

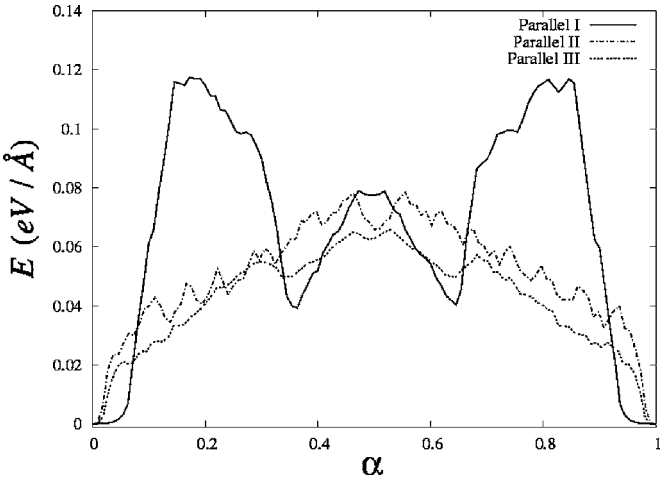

FIG. 11. The minimum-energy paths for the migration of the surface dislocation in the direction parallel to the dislocation line. "Parallel I," "parallel II," and "parallel III" correspond to the atomic motions shown in Figs. 8(c)–8(e), respectively.

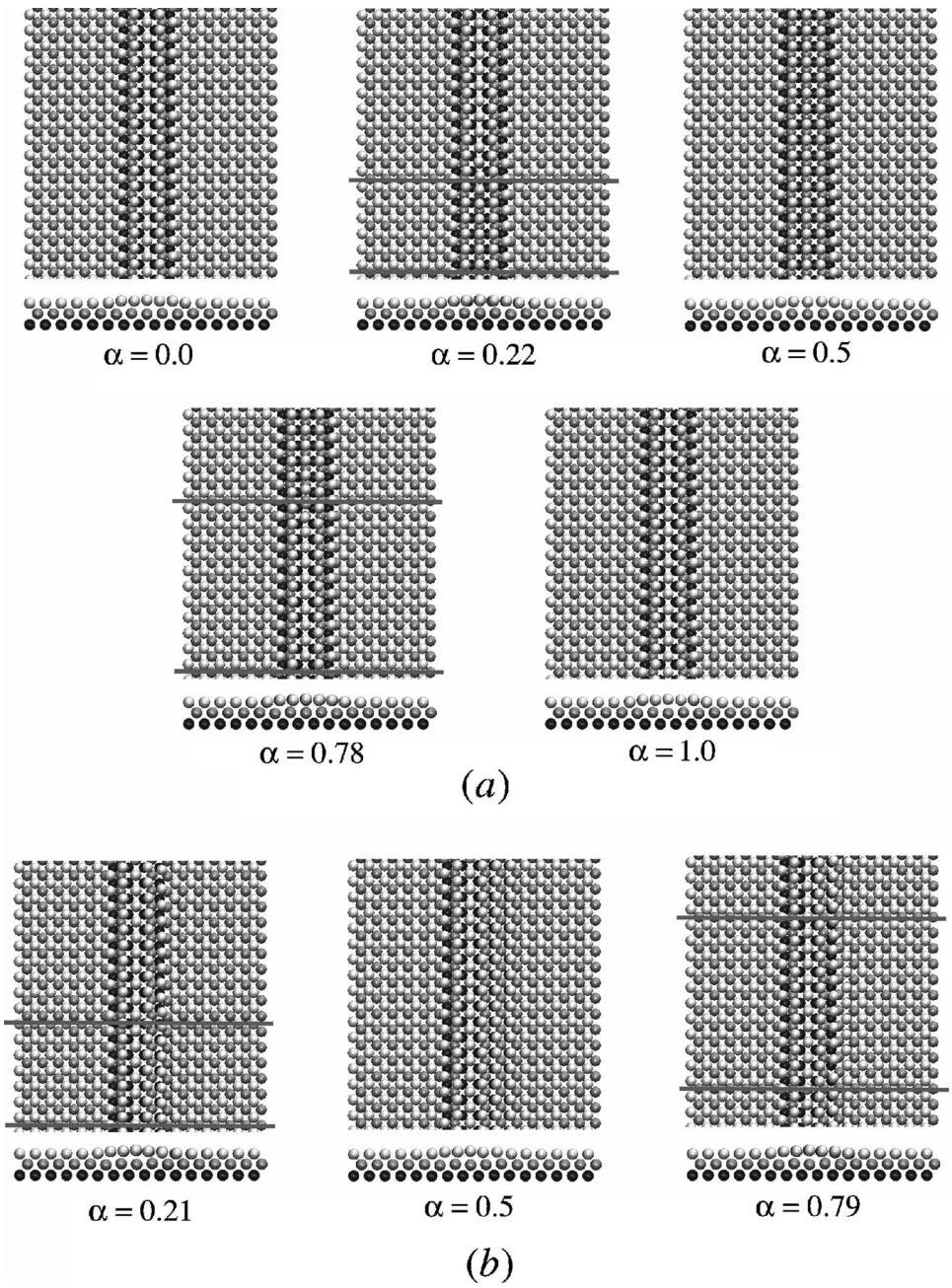

FIG. 12. Representative atomic structure images during the migration of surface dislocations: (a) parallel II and (b) parallel III motions. In each image pair, the upper one is a top view (i.e., along ⟨001⟩), while the lower one is a side view (along ⟨110⟩). α denotes the reaction coordinate. Note that the initial and final (α=0.0 and 1.0) states of these two types of motion are the same, and therefore these states are not shown in (b). The thick gray lines at α=0.22 and 0.78 in (a) and α=0.21 and 0.79 in (b) highlight the boundaries of different surface atomic packings in the surface dislocation cores.

Figure 12 shows a series of representative atomic structures during parallel II and III motions. In Fig. 12(b), we do not show the initial (α=0) and final (α=1.0) states because they are identical with those in Fig. 12(a). Combining Figs. 11 and 12, we see that α=0.5 corresponds to the activated states for both parallel II and III motions. Note that in the α=0.5 configuration, there are three colinear (in the horizontal direction) light gray atoms, while in the initial α=0 configuration, these three atoms are not colinear. In the α=0.22 configuration, there is a region (between the two thick gray horizontal lines) where the dislocation core structure looks like that of α=0.5, and a coexisting region where the dislocation core structure looks like that of α=0. A similar situation exists for α=0.78 between the final state α=1 and the activated α=0.5 states. The two gray lines indicate for parallel II motion the equivalent of kinks seen in the perpendicular motion. A similar situation exists for the parallel III motion [Fig. 12(b)]. Since in these types of parallel motion the kinks are confined to lie in the surface dislocation line itself, it may be more appropriate to refer to these as solitons

rather than kinks. Nonetheless, all types of surface dislocation motion occur via a nucleation and point defect migration mechanism. It is also interesting to mention that, though the activation energy of parallel I motion is much higher than parallel II and III motions (which implies that parallel I motion is almost impossible to occur), the two metastable transition states of parallel motion I (see Fig. 11), which corresponds to $\alpha=0.37$ and 0.67, are also quite similar with type II surface dislocation.

VI. DISCUSSION

We have employed atomistic simulation methods with a MEAM potential for Au to examine the structure, thermodynamics, and migration of surface dislocations on Au (001). We observe two stable surface dislocation structures: type I and II surface dislocations. The existence and core structures of these two surface dislocation types are in good agreement with previous experimental observations.[13,15] We examined how the Au (001) surface energy and surface stress are influenced by the presence of these two types of surface dislocations as a function of surface dislocation separation d. We found that type I surface dislocations tend to attract each other at large separations (in agreement with experiment[13]). Type I surface dislocation separation that corresponds to the lowest surface energy is equivalent to the (5×1) reconstructed surface of Au (001) (also in agreement with experiments[2,4,7,8]). Our calculations also show that adatoms on Au (001) surface will spontaneously be injected into the surface atomic plane but that this injection is thermally activated and hence will only occur at finite temperature. The injection of adatoms to form surface dislocations was observed using HREM by Zandbergen *et al.*[15]

The effect of surface dislocations on the surface stress is somewhat counterintuitive. Since the formation of a surface dislocation requires the injection of an extra atomic column into the (001) surface atomic plane, we would expect surface dislocation injection to make the surface stress more compressive (or, at least, less tensile). This is exactly what we observed for type II surface dislocation. However, injecting the energetically more favorable type I surface dislocation in the Au (001) surface atomic plane makes the tensile surface stress even more tensile. If we compare the displacement field of these two types of surface dislocations (Figs. 5 and 6), we see that type I surface dislocation attracts neighboring surface atoms, while type II surface dislocation repels them. This is consistent with our surface stress change observations. By careful examination of how surface atoms are displaced during the formation of both types of surface dislocations (see Fig. 7), we understand that the differences in surface atomic packings of type I and II surface dislocation are responsible for the differences observed in the displacement fields.

The fact that type I surface dislocation makes the Au (001) surface more tensile implies that the formation of surface dislocations is not the cause of the compressive stresses often measured during the growth of continuous film.[16] Therefore, other yet unknown mechanisms are probably responsible for this phenomena. Furthermore, it has long been believed that the presence of a large tensile surface stress on Au (001) leads to the (5×1) reconstruction; i.e., the reconstruction relaxes the large tensile surface stress.[28] However, our calculations clearly show that the introduction of the stable type I form of surface dislocations that make up the observed (5×1) reconstructions does not reduce the surface stress. Quite the contrary, the reconstruction raises the surface stress. Therefore, relaxation of the large tensile surface stress cannot explain the surface reconstruction of Au (001). Nonetheless, introduction of type I surface dislocations does reduce the energy of the system and, hence, is the source of the surface reconstruction.

We have also obtained the activation energies of surface dislocation migration both perpendicular and parallel to the surface dislocation line direction (using the string method). We found that all transitions from one state to another are achieved by a kink or soliton formation and/or propagation mechanism. Table I shows that the canted and parallel I motions have much higher activation energies and therefore will likely not occur. Parallel II and parallel III and the perpendicular types of motion all have a similar, low activation energy, 0.07 eV/Å. Therefore, surface dislocation motion parallel and perpendicular to the line direction should readily occur. Both types of motion have been observed experimentally,[13–15] consistent with our simulations.

Surface dislocations may play an important role in mass transport on Au (001). Conventionally, surface mass transport on metal surfaces is thought to occur via hopping or exchange mechanisms. More recently, evidence has accumulated that suggests that a surface crowdion mechanism may be favorable; e.g., see the work on strained Cu (001).[29] Since the surface dislocation is more stable than a random array of crowdions in the surface plane and because the surface dislocation can migrate either perpendicular or parallel to the line direction, it is reasonable to speculate that surface dislocations may play an important role in mass transport on the Au (001) surface. This mechanism may be particularly important during film growth, where the Au (001) surface is not fully reconstructed. The HREM observations of Zandbergen *et al.*[15] suggest that the motion of a surface dislocation in the parallel direction may provide a mechanism by which atoms can be transported through a surface step onto a lower-lying terrace. Our calculation results suggest that the low activation energy for surface dislocation migration parallel to its line direction makes this type of motion posible. This may provide an alternative path for an adatom to cross from one terrace to another that is energetically more favorable than the direct step crossing because of the high Ehrlich-Schwoebol barrier.[30,31] In such a model, adatoms inject into the surface to become a part of a surface dislocation, which can in turn migrate parallel to the line direction, and eject the extra adatom onto a lower terrace when the dislocation intersects a step. Since we have not considered the interaction of surface dislocations with steps, this suggestion is speculative.

Finally, since Au (001) is not the only metal surface to have a surface dislocation type of equilibrium reconstruction, it is possible that highly mobile surface dislocations will occur on a wide variety of other surfaces and metals. We note that the surface reconstructions of the (001) surfaces of Pt and Ir are very similar to the Au (001) surface studied here

and hence would be an obvious place to look first. It is also possible that surface dislocations exist on surfaces other than (001), provided that the surface atom density on these unreconstructed surfaces is lower than on the reconstructed surfaces [e.g.,(111) surfaces of many transition metals are in this category]. Therefore, the present results hint at the existence of a relatively common model of surface defects and surface transport that is relatively unexplored–either in experiment or in theory.

VII. CONCLUSION

We have examined both the thermodynamic and kinetic properties of highly mobile surface dislocations on Au (001) using atomistic scale simulations. Two types of surface dislocation structures were found and shown to correspond well with experimental observations. We also calculated the energy γ of (001) surfaces with each type of surface dislocation as a function of surface dislocation separation d. In both cases, the presence of surface dislocations reduces the surface energy and therefore is more stable relative to the unreconstructed (001) surface and that with adatoms. This too is consistent with experimental observations. The lowest surface energy obtained corresponds to a surface with a (5×1) surface reconstruction, which is consistent with previous studies on surface reconstruction of Au. The surface stress f as a function of dislocation separation d was also determined. Type II surface dislocations dramatically reduce the surface stress of Au (001), whereas type I surface dislocations increase the surface stress; this is surprising in light of the expectation that inserting an extra column of atoms into the surface plane will lead to a less tensile surface. Examination of displacement fields shows that the surface atoms outside the dislocation core are attracted toward the dislocation core due to type I surface dislocation core structure, and therefore the surface is stretched near type I surface dislocation (leading to an increase in the tensile surface stress). Our surface stress results also reveal that relaxation of large tensile surface stress might not be the driving force of surface reconstruction. The activation energy for surface dislocation migration along directions perpendicular or parallel to the dislocation line direction was determined using the string method. Our calculations show that the activation energy for migration is sensitive to the detailed translation path. We were able to identify the likely migration path for motion both parallel and perpendicular to the line direction. We found that dislocation motion perpendicular to the line direction occurs through a kink formation and/or propagation mechanism. The translation path for type I surface dislocation perpendicular to its line directions passes through the metastable type II surface dislocation structure. The observation that there are low activation surface dislocation translation paths in both perpendicular and parallel to the line directions suggests that both types of motion occur. In fact, both have been observed experimentally. Finally, our simulations suggest that highly mobile surface dislocations can provide a preferred mechanism for surface mass transport.

[1] M. A. Vanhove, R. J. Koestner, P. C. Stair, J. P. Biberian, L. L. Kesmodel, I. Bartos, and G. A. Somorjai, Surf. Sci. **103**, 218 (1981).

[2] M. A. Vanhove, R. J. Koestner, P. C. Stair, J. P. Biberian, L. L. Kesmodel, I. Bartos, and G. A. Somorjai, Surf. Sci. **103**, 189 (1981).

[3] K. Takayanagi and K. Yagi, Trans. Jpn. Inst. Met. **24**, 337 (1983).

[4] G. K. Binnig, H. Rohrer, C. Gerber, and E. Stoll, Surf. Sci. **144**, 321 (1984).

[5] U. Harten, A. M. Lahee, J. P. Toennies, and C. Woll, Phys. Rev. Lett. **54**, 2619 (1985).

[6] J. V. Barth, H. Brune, G. Ertl, and R. J. Behm, Phys. Rev. B **42**, 9307 (1990).

[7] B. M. Ocko, D. Gibbs, K. G. Huang, D. M. Zehner, and S. G. J. Mochrie, Phys. Rev. B **44**, 6429 (1991).

[8] D. M. Zehner, S. G. J. Mochrie, B. M. Ocko, and D. Gibbs, J. Vac. Sci. Technol. A **9**, 1861 (1991).

[9] A. R. Sandy, S. G. J. Mochrie, D. M. Zehner, G. Grubel, K. G. Huang, and D. Gibbs, Phys. Rev. Lett. **68**, 2192 (1992).

[10] D. L. Abernathy, D. Gibbs, G. Grubel, K. G. Huang, S. G. J. Mochrie, A. R. Sandy, and D. M. Zehner, Science **283**, 260 (1993).

[11] M. Bott, M. Hohage, T. Michely, and G. Comsa, Phys. Rev. Lett. **70**, 1489 (1993).

[12] G. Ritz, M. Schmid, P. Varga, A. Borg, and M. Ronning, Phys. Rev. B **56**, 10518 (1997).

[13] M. Labayen, C. Ramirez, W. Schattke, and O. M. Magnussen, Nat. Mater. **2**, 783 (2003).

[14] M. Labayen, C. Haak, and O. M. Magnussen, Phys. Rev. B **71**, 241409(R) (2005).

[15] H. W. Zandbergen, C. W. Pao, and D. J. Srolovitz, Phys. Rev. Lett. **98**, 036103 (2007).

[16] J. A. Floro, S. J. Hearne, J. A. Hunter, P. Kotula, E. Chason, S. C. Seel, and C. V. Thompson, J. Appl. Phys. **89**, 4886 (2001).

[17] C. Friesen and C. V. Thompson, Phys. Rev. Lett. **93**, 056104 (2004).

[18] F. Ercolessi, M. Parrinello, and E. Tosatti, Surf. Sci. **177**, 314 (1986).

[19] F. Ercolessi, M. Parrinello, and E. Tosatti, Philos. Mag. A **58**, 213 (1988).

[20] M. I. Haftel, Phys. Rev. B **48**, 2611 (1993).

[21] M. I. Haftel and M. Rosen, Phys. Rev. B **64**, 195405 (2001).

[22] M. I. Baskes, Phys. Rev. B **46**, 2727 (1992).

[23] B. J. Lee, J. H. Shim, and M. I. Baskes, Phys. Rev. B **68**, 144112 (2003).

[24] C.-W. Pao, D. J. Srolovitz, and C. V. Thompson, Phys. Rev. B **74**, 155437 (2006).

[25] W. E, W. Ren, and E. Vanden-Eijnden, Phys. Rev. B **66**, 052301 (2002).

[26] There are many local energy minima with almost identical energies for configurations around the initial and final states, and therefore it is difficult to relax the surface dislocation to the

absolute lowest-energy configuration during the energy path calculation. Since these energies are all extremely small, we neglect these small differences here.

[27] M. Finnis and V. Heine, J. Phys. F: Met. Phys. **4**, L37 (1974).

[28] V. Fiorentini, M. Methfessel, and M. Scheffler, Phys. Rev. Lett. **71**, 1051 (1993).

[29] W. Xiao, P. A. Greaney, and D. C. Chrzan, Phys. Rev. Lett. **90**, 156102 (2003).

[30] G. Ehrlich and F. G. Hudda, J. Chem. Phys. **44**, 1039 (1966).

[31] Schwoebe.Rl and E. J. Shipsey, J. Appl. Phys. **37**, 3682 (1966).